

# Evidence for differentiation in the iron-helicoidal-chain in $\text{GdFe}_3(\text{BO}_3)_4$

S.A. Klimin,<sup>1,2</sup> D. Fausti,<sup>1</sup> A. Meetsma,<sup>1</sup> L.N. Bezmaternykh,<sup>3</sup> P.H.M. van Loosdrecht,<sup>1</sup> and T.T.M. Palstra<sup>1</sup>

<sup>1</sup>*Material Science Center, University of Groningen, 9747 AG Groningen, The Netherlands.*

<sup>2</sup>*Institute of Spectroscopy, RAS, 142190, Troitsk, Moscow Region, Russia.*

<sup>3</sup>*L.V. Kirensky Institute of Physics, Siberian branch of RAS, Krasnoyarsk 660036, Russia.*

We report on a single-crystal X-ray structure study of  $\text{GdFe}_3(\text{BO}_3)_4$  at room temperature and at  $T=90$  K. At room temperature  $\text{GdFe}_3(\text{BO}_3)_4$  crystallizes in a trigonal space group  $R\bar{3}2$  (No. 155), the same as found for other members of iron-borate family  $\text{RFe}_3(\text{BO}_3)_4$ . At 90 K the structure of  $\text{GdFe}_3(\text{BO}_3)_4$  transforms to the space group  $P\bar{3}_121$  (No. 152). The low-temperature structure determination gives new insight into the weakly first-order structural phase transition at 156 K and into the related Raman phonon anomalies. The presence of two inequivalent iron chains in the low temperature structure provides a new perspective on the interpretation of the low-temperature magnetic properties.

## I. INTRODUCTION

The family of borates  $\text{RM}_3(\text{BO}_3)_4$  with a rare earth (RE) or yttrium as R and Al, Ga, Fe, or Sc as M crystallize in the huntite,  $\text{CaMg}_3(\text{CO}_3)_4$ , structure type with space group  $R\bar{3}2$ <sup>1,2,3</sup>. The interest in this family of crystals arises both from a fundamental point of view and from already realized and proposed applications. Crystals of  $\text{YAl}_3(\text{BO}_3)_4$  and  $\text{GdAl}_3(\text{BO}_3)_4$  doped with Nd were widely studied during recent years and have been used in optical devices, such as self-frequency doubling and self-frequency summing lasers (see, e.g., Ref.<sup>4</sup> and references therein). Concentrated  $\text{NdAl}_3(\text{BO}_3)_4$  crystals are efficient media for minilasers<sup>5</sup>.

Apart from the interesting optical properties arising chiefly from the lack of inversion symmetry, the 'sub-family' of  $\text{RFe}_3(\text{BO}_3)_4$  also attracts considerable attention due to their structure peculiarities. The presence of magnetic order at temperatures less than 37 K was attributed to magnetic Fe-Fe or Fe-O-Fe interactions inside quasi one-dimensional (1D) iron chains<sup>3,6</sup>. Recent works<sup>6,7</sup>, focusing on low temperature magnetism in  $\text{GdFe}_3(\text{BO}_3)_4$ , revealed two magnetic phase transitions. The second-order magnetic ordering phase transition at  $T_{\text{N}1}=37$  K (antiferromagnetic ordering of Fe atoms) is followed by a first-order spin-reorientational phase transition at  $T_{\text{N}2}=10$  K. Additionally specific heat and Raman measurements on single crystals<sup>7</sup> of  $\text{GdFe}_3(\text{BO}_3)_4$  revealed a weakly first-order structural phase transition at  $T_s=156$  K. This structural phase transition is observed in almost all members of the RE ferro-borates family<sup>7,8,9</sup>. Recently, Hinatsu et al.<sup>8</sup> have shown that  $\text{DyFe}_3(\text{BO}_3)_4$  undergoes such structural phase transition at 340 K, by measuring the temperature dependence of the lattice parameters on powder samples. Here too, a peak in the specific heat was observed at this temperature. Similar peaks in specific heat vs temperature dependence were found for other heavy RE (R= Eu-Ho, Gd, Tb) ferroborates. These peaks were ascribed to structural phase transitions. The transition temperatures  $T_s$  were found to depend linearly on the ionic radius of the RE. To date, there are no single crystal data available nor has the low-temperature (LT) space group been determined.

The high temperature (HT)  $R\bar{3}2$  structure of powder  $\text{RFe}_3(\text{BO}_3)_4$  compounds was first determined in Ref.<sup>1</sup> for R = La, Nd, Sm-Ho, and Y. X-ray experiments on single crystals with R=Nd<sub>0.5</sub>Bi<sub>0.5</sub><sup>2</sup> and R=La, Nd, and Y<sub>0.5</sub>Bi<sub>0.5</sub><sup>3</sup> confirmed this structure. Moreover, Raman measurements for  $\text{LaFe}_3(\text{BO}_3)_4$ <sup>10</sup>,  $\text{NdFe}_3(\text{BO}_3)_4$ <sup>9,10</sup> and  $\text{GdFe}_3(\text{BO}_3)_4$ <sup>9</sup> are in good agreement with group theoretical analysis, based on the  $R\bar{3}2$  structure.

Summarizing, whereas the HT crystal structure of most of the ferroborates is known, the LT space group, lattice parameters, and atomic positions are unknown. In this work we report on a single-crystal X-ray diffraction structure study of gadolinium-iron borate at room temperature (RT) and at 90 K. It is found that the LT-structure has the  $P\bar{3}_121$  symmetry. Two nonequivalent spin chains exist in the LT-structure which gives new insight in the low-temperature magnetic properties. The  $P\bar{3}_121$  symmetry of the LT-phase also confirms the interpretation of the reported IR absorption by crystal-field transitions<sup>7,11</sup> and leads to a better understanding of some peculiarities observed in Raman spectra<sup>7,9</sup>.

## II. EXPERIMENT AND RESULT OF STRUCTURE DETERMINATION

Crystals of  $\text{GdFe}_3(\text{BO}_3)_4$  were grown using a  $\text{K}_2\text{Mo}_3\text{O}_{10}$  - based flux, as described in Ref.<sup>6</sup>. Big transparent single crystals of gadolinium ferroborates were light green in color and had a good optical quality. A block-shaped crystal ('broken-fragment') with the dimensions of  $0.22 \times 0.15 \times 0.11$  mm<sup>3</sup> was mounted on top of a glass fiber and aligned on a Bruker<sup>12</sup> SMART APEX CCD diffractometer. The crystal was cooled to 90(1) K using a Bruker KRYOFLEX. Intensity measurements were performed using graphite monochromated Mo-K $\bar{\alpha}$  radiation. Generator settings were

50 KV/ 40 mA. SMART<sup>12</sup> was used for preliminary determination of the unit cell constants and data collection control. The intensities of reflections of a hemisphere were collected by a combination of 6 sets of exposures (frames). Each set had a different angle for the crystal and each exposure covered a range of 0.3° in  $\omega$ . A total of 3600 frames were collected with an exposure time of 10.0 seconds per frame. The overall data collection time was 16 hours. Data integration and global cell refinement was performed with the program SAINT. The final unit cell was obtained from the xyz centroids of 4767 and 5439 reflections after integration for RT and 90 K, respectively. Intensity data were corrected for Lorentz and polarization effects, scale variation, for decay and absorption (an analytical absorption correction was applied), and reduced to  $F_o^2$ . The program suite SHELXTL was used for space group determination (XPREP).

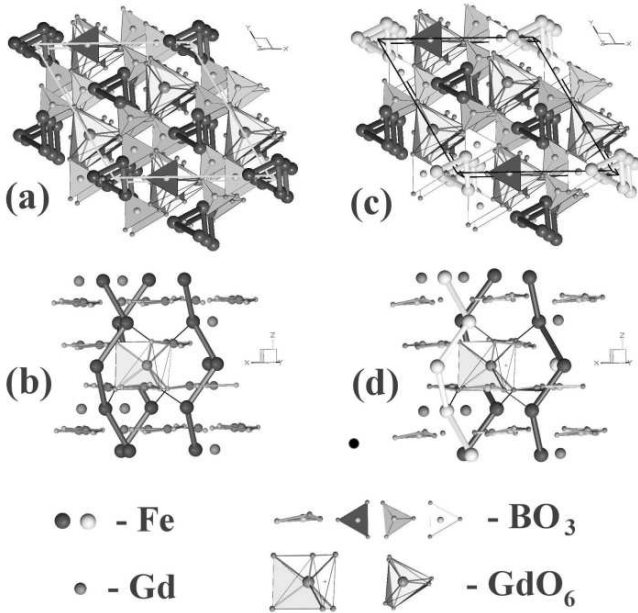


FIG. 1: The structure of GdFe<sub>3</sub>(BO<sub>3</sub>)<sub>4</sub> in two different projection. The left panels (a) and (b) show the RT structure, and the right panels (c) and (d) show the structure at 90 K. The Fe atoms are arranged in chiral chains parallel to the *c*-axis. Different chains are separated by GdO<sub>6</sub> prisms and BO<sub>3</sub> groups. The unit cell outline for *R*32 is shifted by (1/3, 1/3, 0) for comparison with the LT *P*3<sub>1</sub>21 structure.

At both temperatures of RT and 90 K the unit cell was identified as trigonal: reduced cell calculations did not indicate any higher metric lattice symmetry<sup>13</sup>. Space groups *R*32 and *P*3<sub>1</sub>21 were derived for RT and for 90 K, respectively, from the systematic extinctions and discriminated from other candidate space groups, which comply with the same extinctions conditions, during the structure determination process. Examination of the final atomic coordinates of the structure did not yield extra crystallographic or metric symmetry elements<sup>14,15</sup>.

The polarity of the structure of the crystal actually chosen was determined by Flack's *x*-refinement<sup>16,17,18,19</sup>; refinement resulted in a *x* value of 0.50(1), so ultimately an inversion twin is used in the refinement.

Crystal data and numerical details on data collection and refinement are given in Table I. Final fractional atomic coordinates, equivalent displacement parameters and anisotropic displacement parameters are given in Table II for data at RT and in Table III for the 90 K data.

### III. DISCUSSION OF THE STRUCTURE

After a brief introduction describing the main features of GdFe<sub>3</sub>(BO<sub>3</sub>)<sub>4</sub>, we will focus on the difference between the RT and the 90 K (LT) structure. First, we will try to understand the consequences that the structural changes have on the interpretation of Raman spectra anomalies at the weak first-order phase transition reported in the literature<sup>7</sup>. Second, we will give a new perspective for the interpretation of low temperature magnetic data<sup>6,7</sup>.

The room temperature structure of GdFe<sub>3</sub>(BO<sub>3</sub>)<sub>4</sub> belongs to the *R*32 space group (Fig. 1a and 1b). Our measurement confirms the structure reported previously for powder samples<sup>1</sup> and for several single crystals<sup>2,3</sup> from the family RFe<sub>3</sub>(BO<sub>3</sub>)<sub>4</sub>. The structure consists of alternating layers (parallel to *ab*-plane) of Fe-Gd and BO<sub>3</sub> groups (see Fig. 1b). The main features of this structure are already described in literature<sup>3</sup>: the BO<sub>3</sub> groups are arranged in layers

TABLE I: Crystallographic parameters

**a-Crystal data and details of the structure determination.**

Moity Formula	Room Temperature = 293(1) K T = 90(1) K		
Formula Weight (g.mol <sup>-1</sup> )	GdFe <sub>3</sub> (BO <sub>3</sub> ) <sub>4</sub>		
Crystal System	Trigonal		
Space group.	R32, 155	P3 <sub>1</sub> 21, 152	
<i>a</i> (Å)	9.5203(6)	9.5305(3)	
<i>c</i> (Å)	7.5439(5)	7.5479(2)	
<i>V</i> (Å <sup>3</sup> )	592.15(7)	593.73(3)	
Θ range unit cell:min.-max., deg; reflections	3.66-38.70;4767	3.66-38.55; 5439	
Formula <sub>a</sub> Z	3	3	
Space group <sub>a</sub> Z	18	6	
Z' (=Formula <sub>a</sub> Z/SpaceGroup <sub>a</sub> Z)	1/6	0.5	
$\rho$ (g/cm <sup>3</sup> )	4.712	4.699	
F(000) electrons	774	774	
$\mu$ (MoK $\alpha$ )(cm <sup>-1</sup> )	137.74	137.37	

**b-Data collection.**

$\lambda$ (MoK $\alpha$ ), Å	0.71073	
Monochromator	Graphite	
Measurements device type	Bruker SMART APEX, CCD area-detector diffractometer	
Detector area resolution (pixels/mm)	4096 × 4096/62 × 62 (binned 512)	
Measurement method	$\varphi$ - and $\omega$ -scans	
$\theta$ range; min. max.,deg	3.66, 38.70	2.47, 38.58
Index ranges	$h : -16 \rightarrow 16; k : -16 \rightarrow 16; l : -13 \rightarrow 13$	$h : -16 \rightarrow 16; k : -16 \rightarrow 16; l : -13 \rightarrow 13$
Min.- Max. absorption transmission factor	0.0563-0.2519	0.0620-0.2513
X-ray exposure time, h	16.0	16.0
Total data	4700	13868
Unique data	755	2217
Data with criterion: ( $F_O \geq 4.0\sigma(F_O)$ )	755	1956
$R_{int} = \sum [  F_O^2 - F_O^2(means)  ] / \sum [F_O^2]$	0.0339	0.0338
$R_{sig} = \sum \sigma(F_O^2) / [F_O^2]$	0.0203	0.0189
<b>c-Refinement.</b>		
Number of reflections	755	2217
Number of refined parameters	35	95
Isotropic secondary-extinction coefficient, g	0.0371(12)	0.0359(10)
Final agreement factors:	0.0374	0.0452
$wR(F^2) = [\sum [w(F_O^2 - F_c^2)^2] / [w(F_O^2)^2]]^{1/2}$		
Weighting scheme: a, b	0.0272, 0.0	0.0312, 0.0
$w = 1 / [\sigma^2(F_O^2) + (aP)^2 + bP]$		
And $P = [max(F_O^2, 0) + 2F_c^2]/3$		
$R(F) = \sum (  F_O  -  F_c  ) / \sum  F_O $ for $F_O > 4.0\sigma(F_O)$	0.0151	0.0167
Absolute-Structure parameter Flack's x	0.50	0.50
$GooF = S = [\sum [w(F_O^2 - F_c^2)^2] / (n - p)]^{1/2}$	1.075	0.855
<i>n</i> = number of reflections		
<i>p</i> = number of parameters refined		
Residual electron density in final	-1.0, 0.6(1)	-0.5, 0.8(1)
Difference Fourier map, e/Å <sup>3</sup>		
Max. (shift/s) final cycle	0.001	0.003
Average (shift/ $\sigma$ ) final cycle	0.000	0.000

TABLE II: Fractional atomic coordinates and Anisotropic Parameters at RT

Atom	Wyckoff	Schoenflies	x	y	z	$U_{eq}$ (Å)
Gd	3 a	D <sub>3</sub>	0	0	0	0.00867(5)
Fe	9 d	C <sub>2</sub>	0.21659(5)	1/3	1/3	0.00654(9)
O1	9 e	C <sub>2</sub>	0.1442(2)	x	1/2	0.0083(3)
O2	9 e	C <sub>2</sub>	0.4087(3)	x	1/2	0.0132(5)
O3	18 f	C <sub>1</sub>	0.0254(2)	0.2125(2)	0.1824(2)	0.0095(3)
B1	3 b	D <sub>3</sub>	0	0	1/2	0.0066(6)
B2	9 e	C <sub>2</sub>	0.5526(3)	x	1/2	0.0077(4)

Atom	$U_{11}$	$U_{22}$	$U_{33}$	$U_{23}$	$U_{13}$	$U_{12}$
Gd	0.00888(8)	0.00888(8)	0.00825(9)	0.0000(-)	0.0000(-)	0.00444(4)
Fe	0.00591(12)	0.00635(14)	0.00750(18)	0.00009(8)	0.00004(4)	0.00317(7)
O1	0.0058(5)	0.0058(5)	0.0109(7)	0.0014(3)	0.0014(3)	0.0011(6)
O2	0.0076(6)	0.0076(6)	0.0182(11)	0.0047(5)	0.0047(5)	0.0009(8)
O3	0.0065(5)	0.0112(5)	0.0111(5)	0.0025(5)	0.0021(4)	0.0046(4)
B1	0.0058(9)	0.0058(9)	0.0081(14)	0.0000(0)	0.0000(-)	0.0029(4)
B2	0.0070(7)	0.0070(7)	0.0093(8)	0.0007(4)	0.0007(4)	0.0036(11)

TABLE III: Fractional atomic coordinates and Anisotropic Parameters at T=90 K

Atom	Wyckoff	Schoenflies	x	y	z	$U_{eq}(\text{\AA})$
Gd	3 a	C <sub>2</sub>	-0.33342(1)	x	0	0.00406(4)
Fe1	3 a	C <sub>2</sub>	0.11536(5)	x	0	0.00360(6)
Fe2	6 c	C <sub>1</sub>	-0.21420(6)	-0.54975(4)	0.34154(2)	0.00366(6)
O1	3 b	C <sub>2</sub>	0	-0.07819(15)	1/6	0.0072(3)
O2	6 c	C <sub>1</sub>	-0.5832(2)	-0.2709(1)	0.13774(12)	0.00692(17)
O3	6 c	C <sub>1</sub>	-0.1194(3)	-0.30445(26)	-0.17980(18)	0.0057(3)
O4	6 c	C <sub>1</sub>	-0.1467(3)	-0.36234(16)	0.18479(18)	0.0058(2)
O5	6 c	C <sub>1</sub>	0.4755(2)	0.1451(2)	-0.15980(8)	0.0057(3)
O6	3 b	C <sub>2</sub>	0.1877(2)	0	5/6	0.0049(3)
O7	6 c	C <sub>1</sub>	-0.5235(3)	-0.53811(17)	-0.18533(18)	0.0056(2)
B2a	6 c	C <sub>1</sub>	-0.4473(4)	-0.1201(-)	0.15617(14)	0.0053(3)
B2b	3 b	C <sub>2</sub>	0	-0.2223(3)	1/6	0.0049(4)
B1	3 b	C <sub>2</sub>	0.33204(14)	0	5/6	0.0045(5)

Atom	$U_{11}$	$U_{22}$	$U_{33}$	$U_{23}$	$U_{13}$	$U_{12}$
Gd	0.00409(6)	0.00409(7)	0.00408(7)	0.00010(2)	0.00009(1)	0.00210(3)
Fe	0.00355(10)	0.00355(10)	0.00355(10)	0.00006(4)	0.00006(4)	0.00166(10)
Fe	0.00349(9)	0.00356(11)	0.00378(9)	0.00013(7)	0.00003(5)	0.00166(6)
O1	0.0081(6)	0.0054(4)	0.0089(4)	0.00121(19)	0.0024(4)	0.0040(3)
O2	0.0058(3)	0.0062(3)	0.081(3)	0.0012(3)	0.0014(3)	0.0025(3)
O3	0.0062(4)	0.0040(5)	0.0065(4)	0.0006(3)	0.0007(3)	0.0023(4)
O4	0.0054(4)	0.0045(4)	0.0067(4)	0.0007(3)	0.0003(3)	0.0019(4)
O5	0.0051(4)	0.0050(4)	0.0063(5)	0.0007(3)	0.0003(3)	0.0019(5)
O6	0.0044(4)	0.0058(6)	0.0062(5)	0.0019(5)	0.0010(2)	0.0029(3)
O7	0.0047(4)	0.0063(4)	0.0064(4)	0.0008(3)	0.0001(3)	0.0033(4)
B2a	0.0050(6)	0.0067(7)	0.0055(5)	0.0004(5)	0.0001(4)	0.0040(4)
B2b	0.0018(8)	0.0061(6)	0.0055(7)	0.0004(3)	0.0008(6)	0.0009(4)
B1	0.0042(8)	0.0048(9)	0.0046(11)	0.0009(5)	0.0004(2)	0.0024(4)

nearly perpendicular to the C<sub>3</sub> axis and the Fe atoms are arranged in helicoidal chains parallel to this axis. Different chains are connected by GdO<sub>6</sub> and BO<sub>3</sub> groups, where each individual BO<sub>3</sub> and GdO<sub>6</sub> group connects three chains. The distance between Fe atoms in the same chain (3.1669(4) Å) is shorter than the Fe-Fe distances for two nearest chains, that varies along the chain, 4.8308(5) Å, being the shortest one. The main exchange interaction between Fe<sup>3+</sup> is therefore of quasi-1D nature.

TABLE IV: Symmetry position of BO<sub>3</sub> groups, angle between the group and the *c*-axis and their flatness of them. The flatness is expressed as distance of the B atoms from the plane defined by the three oxygen ligands.

Room Temperature			Low Temperature		
	Symm. Angle [degr.]	Flatness		Symm. Angle [degr.]	Flatness
B1	D <sub>3</sub>	90	0	B1	C <sub>2</sub>
B2	C <sub>2</sub>	84.37(11)	0	B2a	C <sub>1</sub>
				B2b	C <sub>2</sub>
					87.52(4) 0.00002(4)
					81.89 0.0055(11)
					83.55 0.0000(2)

Upon lowering the temperature the GdFe<sub>3</sub>(BO<sub>3</sub>)<sub>4</sub> crystal reduces the symmetry from *R*32 to *P*3<sub>1</sub>21, in the trigonal system. Fig. 2 shows the coordination polyhedra (GdO<sub>6</sub>, FeO<sub>6</sub>, and BO<sub>3</sub>) for two different structures *R*32 and *P*3<sub>1</sub>21. At RT the BO<sub>3</sub> groups occupy two inequivalent positions, B1 (D<sub>3</sub>) and B2 (C<sub>2</sub>). At 90 K the site symmetry of the B1 atoms is reduced to C<sub>2</sub>, whereas the site symmetry of the B2 atoms differentiates into a B2b (C<sub>2</sub>) and B2a (C<sub>1</sub>) (see also Table IV). In the LT-phase, the angle between BO<sub>3</sub> groups and *c*-axis is changed. Moreover, in the LT-phase the BO<sub>3</sub> groups in C<sub>1</sub> position are considerably distorted and no longer flat (see Tab.IV).

The LT structure is in agreement with the Raman data<sup>7,9</sup>. The group theoretical vibrational analysis, based on the 90 K structure, shows that, due to the lowering of the symmetry, new librational modes of the BO<sub>3</sub> become Raman active ( $R_x$  and  $R_y$ ). The observed structural change is compatible with an appearance of the librational  $R_y$  mode of the BO<sub>3</sub> group upon approaching  $T_s$  from above, and a subsequent hardening of this mode in the LT phase (See Fig.3). Also the anisotropic displacement parameters (Table II)  $U_{33}$  of the oxygen atoms suggest that the borate groups are relatively free to oscillate around the *y*-axis.

Concerning the magnetic structure, the main peculiarity of both the RT and the 90 K structures is the existence of

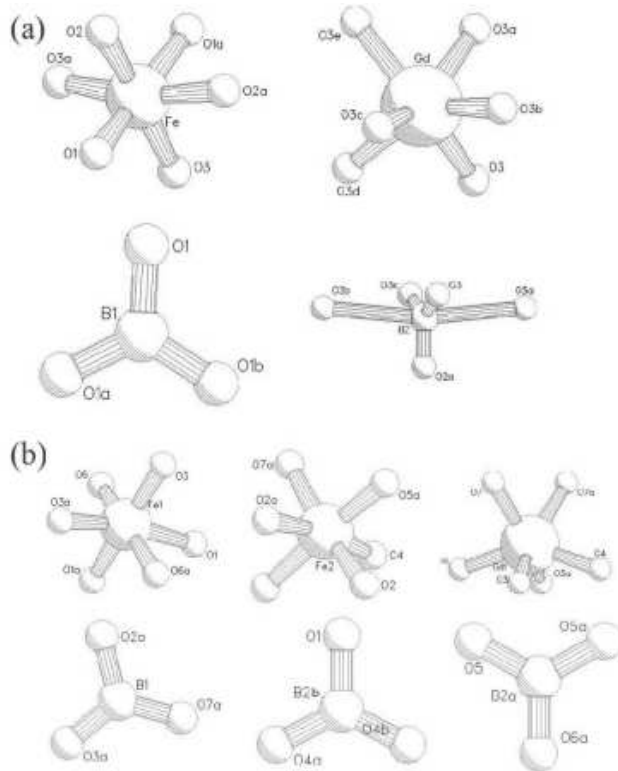


FIG. 2: Coordination polyhedra for the RT ( $R\bar{3}2$ -(a)) and the LT ( $P\bar{3}121$ -(b)) structures of  $\text{GdFe}_3(\text{BO}_3)_4$ . At RT the Fe atoms with  $C_2$ -symmetry are coordinated by three different types of oxygen atoms. At 90 K there are two inequivalent positions for the Fe atoms: Fe1 (the same symmetry as RT) and Fe2, which is in a general position (surrounded by five different types of oxygen). At RT the Gd atoms are surrounded by six oxygens of one type ( $D_3$ -symmetry). At 90 K they are coordinated by three different types of oxygen atoms ( $C_2$ -symmetry). For the B atoms there are two kinds of coordination at RT. B1 (in  $D_3$ -symmetry) is surrounded by three oxygen atoms of the same type, the  $\text{B}_1\text{O}_3$ -group is thus an equilateral triangle. The B2 atoms are surrounded by two types of O,  $\text{B}_2\text{O}_3$  is an isosceles triangle ( $C_2$ -symmetry). At 90 K there are three kinds of coordinations for the B atoms:  $\text{B}_2\text{bO}_3$  and  $\text{B}_1\text{O}_3$  are isosceles triangles ( $C_2$  symmetry) and  $\text{B}_2\text{aO}_3$  is general triangle.

magnetically quasi-1D helicoidal iron chains (see Fig. 1). The intra-chain exchange interaction between the Fe ions is expected to be dominated by Fe-Fe direct exchange and Fe-O-Fe superexchange, depending respectively on Fe-Fe distance and two Fe-O-Fe angles (Fig.4). Nevertheless there are some significant differences.

At RT all the Fe atoms are in equivalent positions ( $C_2$ ). All Fe-chains are equivalent as are the Fe-O-Fe angles ( $102.40^\circ(12)$  and  $103.65^\circ(8)$ ) and Fe-Fe distances ( $3.1669(4)$  Å). Therefore, the exchange interactions between neighboring iron ions within a chain are also equivalent. At LT (Fig. 1), as shown in Table IV, the  $\text{BO}_3$  groups form one general triangle (gray  $C_1$  position) and two isosceles triangles (white and dark,  $C_2$  position). At RT "gray" and "white" groups become also equivalent, with  $C_2$  symmetry, and the "dark" one is a regular triangle with the  $D_3$  symmetry. The reduction of the symmetry of the borate groups changes the surrounding of the Fe atoms (Fig. 2), yielding two inequivalent positions ( $C_2$  and  $C_1$ ). Therefore, the Fe-Fe distances are different for the two chains: one is stretched ( $3.1828(4)$  Å) and in the other one is compressed ( $3.1554(4)$  Å). The angles Fe-O-Fe for the first chain are  $101.24^\circ(5)$  and  $103.71^\circ(9)$ , while those for the second are  $102.46^\circ(6)$  and  $103.91^\circ(8)$ . Therefore also the intra-chain exchange interaction is different for the two chains.

The  $\text{GdO}_6$  prism connects three chains, one containing Fe1-atoms with  $C_2$  symmetry and two with Fe2-atoms in a general position. There is only one inequivalent position for the Gd-ions in both the RT and the 90 K structures. However, the site symmetry of the Gd-ions changes from  $D_3$  at RT to  $C_2$  at 90 K. This confirms the interpretation of the authors of Ref.<sup>7</sup>, who interpreted low-temperature infrared spectra of  $\text{Nd}_{0.01}\text{Gd}_{0.99}\text{Fe}_3(\text{BO}_3)_4$  in terms of Kramers doublets of Nd, assuming only one structural position for the Nd ions.

The detailed structure of the Fe-chains and their interconnection are shown in Fig. 4. The intra-chain interactions between Fe-atoms go through two Fe-O-Fe superexchange pathways. The magnetic inter-chain interaction arises from the Fe-O-O-Fe, and possibly the Fe-O-Gd-O-Fe superexchange path. The role of the first superexchange path is important because the substitution of Gd for non-magnetic Y does not lead to a disappearance of 3D magnetic

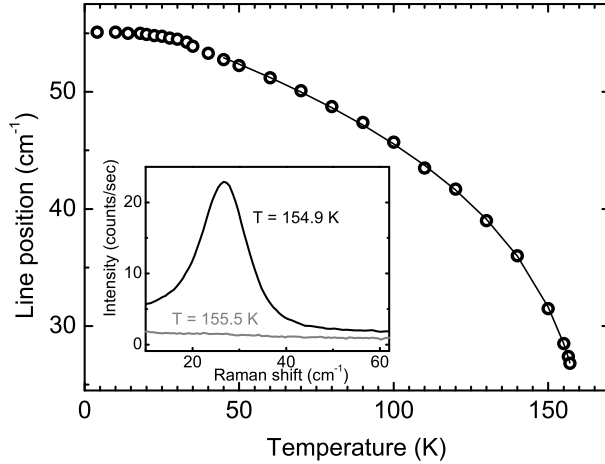


FIG. 3: Temperature dependence of Raman frequency of the low energy mode appearing at the structural phase transition  $T_s$ . Insert shows the low-frequency part of Raman spectrum at two close temperatures before and after phase transition.

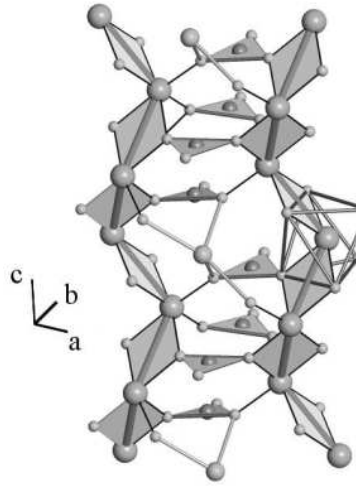


FIG. 4: Two Fe-chains and the most important exchange paths: the intra-chain exchange is via Fe-Fe direct exchange or Fe-O-Fe super-exchange, while the inter-chain exchange is through Fe-O-Gd-O-Fe and Fe-O-O-Fe.

ordering. On the contrary, the Néel temperature for  $\text{YFe}_3(\text{BO}_3)_4$ ,  $T_{\text{N}1}=40$  K, is larger than the one found for Gd-compound ( $T_{\text{N}1}=37$  K), and for  $\text{NdFe}_3(\text{BO}_3)_4$  ( $T_{\text{N}1}=30$  K)<sup>9,11</sup>. Considering the different  $\text{RE}^{3+}$  ionic radii (0.983 Å for Nd, 0.938 Å for Gd, and 0.900 Å for Y) it is clear that the Néel temperature of  $\text{RFe}_3(\text{BO}_3)_4$  depends strongly on the ionic radii: a smaller ionic radius results in a higher  $T_{\text{N}1}$ . Moreover,  $T_{\text{N}1}$  does not seem to be affected by the spin of the RE. In this sense it is clear that the main superexchange path of the interaction between different chains is the Fe-O-O-Fe path, and that a small distortion of this path changes substantially the magnetic properties of the system. It is therefore clear that the existence of two nonequivalent Fe chains with different Fe-Fe distances and Fe-O-Fe angles could lead to substantially different intra-chain exchange constant for the two chains<sup>20</sup>, therefore it should be taken into account for the interpretation of the magnetic properties.

#### IV. CONCLUSIONS

In summary, we have determined the crystal structure of  $\text{GdFe}_3(\text{BO}_3)_4$  at RT and 90 K. At RT  $\text{GdFe}_3(\text{BO}_3)_4$  exhibits  $R\bar{3}2$  structure, in agreement with Refs.<sup>1,3</sup>. Below the structural phase transition ( $T_s = 156$  K) the structure

has the  $P3_121$  space group. The main difference of LT-structure compared to the RT one is the lowering of the symmetry and the tilt of the  $BO_3$  groups. This confirms the interpretation of the Raman spectra of this phase transition. The main conclusion resulting from the LT structure determination is the presence of two inequivalent positions for the Fe atoms giving rise to two different iron helicoidal chains.

## V. ACKNOWLEDGMENTS

The authors are very grateful to M.N. Popova for valuable discussions. This work was partially supported by the Stichting voor Fundamenteel Onderzoek der Materie (FOM, financially supported by the Nederlandse Organisatie voor Wetenschappelijk Onderzoek (NWO)). One of the authors (S.K.) acknowledges the support of the Russian Foundation for Basic Research, grant 04-02-17346, and the Russian Academy of Sciences under the Programs for Basic Research.

---

<sup>1</sup> J. C. Joubert, W. White, and R. Roy, *Appl. Cryst.* **1**, 318 (1968).

<sup>2</sup> E. L. Belokoneva, L. I. Alshinskaya, M. A. Simonov, N. I. Leonyuk, T. I. Timchenko, and N. B. Belov, *Journal structurnoi khimi (Russian Journal of Structural Chemistry)* **20**, 542 (1979).

<sup>3</sup> J. Campá, C. Cascales, E. Gutierrez-Puebla, M. Monge, I. Rasines, and C. Ruiz-Valero, *Chem. Mater.* **9**, 237 (1997).

<sup>4</sup> A. Brenier, C. Tu, Z. Zhu, and B. Wu, *Appl. Phys. Lett.* **84**, 2034 (2004).

<sup>5</sup> X. Chen, Z. Luo, and D. Jaque, *J. Phys.: Condens. Matter.* **13**, 1171 (2001).

<sup>6</sup> A. D. Balaev, L. N. Bezmaternykh, I. A. Gudim, V. L. Temerov, S. G. Ovchinnikov, and S. A. Kharlamova, *J. Magn. Magn. Mater.* **532**, 258 (2003).

<sup>7</sup> R. Z. Levitin, E. A. Popova, R. M. Chtsherbov, A. N. Vasiliev, M. N. Popova, E. P. Chukalina, S. A. Klimin, P. H. M. van Loosdrecht, D. Fausti, and L. N. Bezmaternykh, *JETP Lett.* **79**, 423 (2004).

<sup>8</sup> Y. Hinatsu, Y. Doi, K. Ito, M. Wakushima, and A. Alemi, *J. Solid State Chem.* **172**, 438 (2003).

<sup>9</sup> D. Fausti, S. A. Klimin, and P. H. M. van Loosdrecht (2005), unpublished.

<sup>10</sup> A. De Andres, F. Agullo-Rueda, S. Taboada, C. Cascales, J. Camp, C. Ruiz-Valero, and I. Rasines, *J. Alloys Comp.* **250**, 396 (1997).

<sup>11</sup> E. P. Chukalina, D. Y. Kuritsin, M. N. Popova, L. N. Bezmaternykh, S. A. Kharlamova, and V. L. Temerov, *Phys. Lett. A* **322**, 239 (2004).

<sup>12</sup> Bruker, SMART, SAINT, SADABS, XPREP and SHELXTL/NT. Area Detector Control and Integration Software. Smart Apex Software Reference Manuals. Bruker Analytical X-ray Instruments. Inc., Madison, Wisconsin, USA (2000).

<sup>13</sup> A. L. Spek, *J. Appl. Cryst.* **21**, 578 (1988).

<sup>14</sup> Y. Le Page, *J. Appl. Cryst.* **20**, 264 (1987).

<sup>15</sup> Y. Le Page, *J. Appl. Cryst.* **21**, 983 (1988).

<sup>16</sup> H. D. Flack, *Acta Cryst. A* **39**, 876 (1983).

<sup>17</sup> H. D. Flack and G. Berardinelli, *Acta Cryst. A* **55**, 908 (1999).

<sup>18</sup> H. D. Flack and G. Berardinelli, *Acta Cryst. A* **33**, 1143 (2000).

<sup>19</sup> R. Herbst-Irmer and G. M. Sheldrick, *Acta Cryst. B* **54**, 443 (1998).

<sup>20</sup> J. B. Goodenough, *Phys. Rev.* **100**, 564 (1955).